Supplementary Information for

Satellite Observations Reveal Extreme Methane Leakage from a Natural Gas Well Blowout

Sudhanshu Pandey[1,5], Ritesh Gautam[2], Sander Houweling [1,3], Hugo Denier van der Gon[4], Pankaj Sadavarte[1,4] Tobias Borsdorff [1], Otto Hasekamp[1], Jochen Landgraf[1], Paul Tol[1], Tim van Kempen[1], Ruud Hoogeveen[1], Richard van Hees[1], Steven P. Hamburg[2], Joannes D. Maasakkers[1] and Ilse Aben[1]

(1) SRON Netherlands Institute for Space Research, Utrecht, 3584 CA, the Netherlands,
(2) Environmental Defense Fund, New York, NY 10010, USA USA,
(3) Department of Earth Sciences, Vrije Universiteit Amsterdam, Amsterdam, 1081 HV, the Netherlands,
(4) Department of Climate, Air and Sustainability, TNO, Utrecht, 3584 CB, the Netherlands
(5) Institute for Marine and Atmospheric Research Utrecht, Utrecht University, Utrecht, 3584 CC, The Netherlands

Correspondence to: s.pandey@sron.nl

This PDF file includes:

Supplementary Text
Figs. S1 to S10
Table S1 to S2
Captions for Movie S1

www.pnas.org/cgi/doi/10.1073/pnas.1908712116

Supplementary Text

Section 1: Emission uncertainty quantification

The total uncertainty (σ_{total}) of the emissions rate Q_T estimated using the mass balance approach of *Methods* 3 is quantified as follows:

$$\sigma_{\text{total}} = \sqrt{\sigma^2_{\text{meteo}} + \sigma^2_{\text{sampling}} + \sigma^2_{\text{precision}} + \sigma^2_{\text{method}}} \quad \text{………………………(S1)}$$

Here, σ_{meteo} is the uncertainty of Q_T due to the error in WRF-simulated meteorology. σ_{sampling} is the uncertainty of Q_T due to the spatial sampling of TROPOMI XCH_4 on 27 February 2018, and $\sigma_{\text{precision}}$ is the uncertainty due to precision of TROPOMI XCH_4 retrievals. σ_{method} is the uncertainty of the emission quantification method.

To quantify σ_{meteo}, WRF XCH_4 is sampled at six hourly time instances before and after the TROPOMI overpass time (17:35 UTC). The WRF XCH_4 output for each time instance is then interpolated and re-gridded to the TROPOMI measurement pixels (see Fig. S3), which are then used to generate multiple emission estimates (see Table S1) resulting in a σ_{meteo} of 14 t/hr. Note that σ_{meteo} accounts for inaccuracies in the time interpolation as well as the temporal representation of meteorological variations, including wind speed and direction, in the WRF simulations. σ_{sampling} was calculated by bootstrapping the emission-influenced and background pixels. 10,000 instances of half the number of emission-influenced pixels (=15) and background pixels (=5) were randomly selected and used to calculate 10,000 Q_T values. The spread of these Q_w is σ_{sampling} = 25 t/hr. $\sigma_{\text{precision}}$ is the error on the Q_T due to precision error of individual TROPOMI XCH_4 retrievals in the emission-influenced and background regions. Note that the precision error represents the influence of the radiance measurement noise on TROPOMI XCH_4. (provided as *XCH4_precision* in TROPOMI data products, see Hu et al., *28*). By propagating the precision error of the measurements, we find $\sigma_{\text{precision}}$= 3.2 t/hr. σ_{method} is taken as the 1 standard deviation of mean emission rate estimates from 4 different approaches: 1. mass balance method with 1-band retrievals (see *Methods* 3); 2. cross-sectional flux (CSF) method with 1-band retrievals (SI Section 2); 3. slope method (SI Section 3) with 1-band retrievals; 3. mass balance method with 2-band retrievals (SI Section 4). The σ_{method} is found to be 13 t/hr. Finally, using Equation S1, we calculate σ_{total} = 32 t/hr.

Our WRF simulation is nudged to NCEP meteorological fields. To ensure that we are not underestimating σ_{meteo} by sampling output of a single meteorological model at multiple time steps, we consider the instantaneous wind speed at 10-meter height U_{10} in the blowout region from two additional meteorological models (see Table S2). Varon et al. (*1*) derived the empirical relation between U_{10} and effective wind speed U_{eff} for the integrated mass enhancement (IME) method ($U_{eff} = a\ \log U_{10} + 0.6,\ a = 1.0 \pm 0.1\ \text{ms}^{-1}$) and CSF method ($U_{eff} = b\ U_{10},\ b = 1.4 \pm 0.1$). Note that the IME method of Varon et al. (*1*) is similar to mass balance method used in this study. In both CSF and IME methods, the emission estimate Q is directly proportional to the U_{eff}. The U_{10} of NCEP, ERA-5 and ERA-interim have a 1 standard deviation of 0.2 ms^{-1}. This 7% error on U_{10} translates to 10 % error on CSF's U_{eff}, and 6% error on mass balance's U_{eff}. These errors are lower than σ_{meteo} (= 12%) providing further confidence that we are not underestimating the meteorological error.

Section 2: Emission quantification using the CSF method

As an alternative to the area-integral-based mass balance approach (see *Methods* 3), we also use the cross-sectional flux (CSF) method as described in Varon et al. *(1)* to quantity the blowout emission rate. In this method, the measurement-derived emission rate Q of an isolated point source is quantified using the line-integral mass balance technique along a transect across the plume:

$$C = \int_{-\infty}^{+\infty} \Delta\Omega\,(x\,,y)\,dy \quad \text{...........(S2)}$$

$$Q = CU_{eff} \quad \text{....... (S3)}$$

where C is the tracer enhancement integrated along the transect line (in the y direction), perpendicular to the wind direction (blowing in the x direction), over the detectable width of the plume. U_{eff} is the effective wind speed at which column averaged CH_4 is transported at the location of the transect line. $\Delta\Omega$ is the XCH_4 enhancement relative to an upwind background for a given measurement along the transect. This method can be applied to multiple transect lines at different distances downwind of the source resulting in multiple estimates of Q. These estimates can be used to derive error characteristics of Q

We made 20 transect lines downwind of the blowout location and perpendicular to the local wind direction (see Fig. S4). The upwind background is the same as used for the mass balance method. For each pixel intersecting a transect line, the product of $\Delta\Omega$, and the length of intersection of the transect lines and the pixel was calculated. These numbers were added and multiplied by the U which was calculated from the WRF XCH_4 output: for the blowout tracer, emission rate Q_w is known and the line integrals C_w for each transect line can be calculated from the corresponding XCH_4 output. The ratio between Q_w and the error weighted average of C_w gives U_{eff} = 5.2 m s^{-1}. Using the empirically derived relation ($U_{eff} = bU_{10}$, $b =$ 1.4 $\pm$ 0.1) given in Varon et al. *(1)* and U_{10} from NCEP-FNL (see Table S2), which is used as meteorological boundary condition in WRF, we calculate U_{eff} = 4.4 ± 0.5 m s^{-1}. This U_{eff} is slightly smaller than WRF-derived U_{eff}. In line with Varon et al. *(1)*, we assume a 40% uncertainty on U_{eff}. Note that calculating C_w on the WRF XCH_4 regridded TROPOMI pixels also accounts for the bias introduced applying the mass-balance method to coarse resolution TROPOMI measurements.

The Q values calculated for the transect lines in Fig. S4 are shown in Fig. S5. The error-weighted average of these Q values is 130± 28 t/hr. The uncertainty σ_{total} of Q is calculated as follows

$$\sigma_{\text{total}} = \sqrt{\sigma^2_{\text{meteo-sampling}} + \sigma^2_{\text{precision}} + \sigma^2_{\text{method}}} \quad \text{.........(S4)}$$

$\sigma_{\text{meteo-sampling}}$ is the combined error due to meteorology and TROPOMI XCH_4 sampling. It is calculated by first estimating Q values for each transect line on WRF XCH_4 using U_{eff} = 5.2 ms^{-1}. The 1 standard deviation of the difference between the Q values of WRF and TROPOMI for all transect lines (red curve in Fig. S5) gives $\sigma_{\text{meteo-sampling}}$. $\sigma_{\text{precision}}$ is the TROPOMI XCH_4 retrieval precision (as in Section 1). σ_{method} = 13 t/hr is the uncertainty due to use of CSF method on 1-band data (as in Section 1). Overall, this method leads to σ_{total} = 28 t/hr.

The variability in Q is in large part due to the TROPOMI sampling and meteorological variability as a similar variability is found for WRF Q values. This is shown in Fig. S5. To facilitate comparison, the WRF Q values shown in Fig. S5 are multiplied with 1.625 so that their mean matches the mean of TROPOMI Q values. The Pearson correlation coefficient between WRF and TROPOMI-derived Q values is 0.77, indicating that 60% of the variability in the TROPOMI Q values can be explained by the TROPOMI sampling, and meteorological effects such as wind variability and changes in boundary layer height, which are simulated in WRF. The rest of the variability could be caused by errors in TROPOMI measurements and/or errors in the WRF-simulated transport.

Section 3: Emission quantification using the slope method

The blowout Emission rate can be estimated using the slope method as in Kort et al. (*2*). By performing linear regression between TROPOMI and WRF XCH_4 (see Fig. S6), we find a slope of 1.23± 0.14. By multiplying this slope with the emission rate of 80 t/hr used in the WRF simulation, emission rate of 98 ± 22 t/hr is calculated. This compares well with our mass balance estimate of 120 ± 32 t/hr. The two methods are not expected to yield the same answer, since the slope method uses WRF and TROPOMI XCH_4 values for each pixel, whereas, the mass balance method uses the difference between averages of background and blowout-influenced pixels resulting in a different weighing.

Section 4: Emission quantification using 2-band retrievals

Here we quantify the emission rate for the blowout using data from the operational 2-band TROPOMI XCH_4 retrievals. We find XCH_4 enhancement in the 2-band retrievals that are similar to the 1-band retrievals during the Ohio blowout. The emission quantification with the 2-band retrievals (*Methods* 3) yields 100 ± 32 t/hr, which is in close agreement with the emission rate estimate from the 1-band retrievals of 120 ± 32. The 1-band and 2-band XCH_4 product differ in the spectral information used to constrain the retrieval (only the 2-band retrieval uses NIR data). Both the 1-band and 2-band TROPOMI XCH_4 products show small striping effects. In this study, neither of the products is corrected for striping effect as the available methods may introduce new errors. We have checked and found that the striping effect in XCH_4 is significantly smaller than the signal associated with the Ohio blowout event. In addition, the sampling error (σ_{sampling}) derived using the bootstrapping method should account for the error due to the striping effect (Section 1).

Section 5: Influence of regular emissions

In our emission quantification method (*Methods* 3), the TROPOMI XCH_4 enhancement (X_T) also includes enhancements due to regular emissions in the blowout-influenced region (see Fig. S7). These emissions are accounted for since the WRF XCH_4 enhancement (X_w) is calculated by taking the sum of the EPA, blowout and boundary tracers. The effect of the regular emission will cancel out in $\frac{X_T}{X_W}$ if the EPA emissions are a good estimate of the anthropogenic emissions. We assess the impact of EPA emissions being an underestimate of the regular emissions in the downwind enhancement region. The XCH_4 enhancement of the EPA tracer (X_W^{epa}) is 1.5 ppb, which is ~5% of X_W (= 27 ppb) for sum of all WRF tracers. If the EPA underestimates the emissions in the blowout-influenced region by a factor of 5, X_w would be 33 ppb ($X_w + 4 \times X_w^{epa}$), resulting in Q_T= 97 t/hr. This estimate is still in statistical agreement with the original emission estimate of 120±32 t/hr, indicating that our results are robust to EPA inventory uncertainties.

Further, we also do a CSF quantification for the same transects lines and background area used for 27 February 2018 (SI Section 2) but for measurements on 28 November 2017, i.e., before the blowout when wind conditions were similar. Then we find a Q of 2 (-2/+7) t/hr, which is well within the estimated uncertainty of Q of 28 t/hr during the blowout. This further supports our finding that the large downwind XCH_4 enhancements along the transects are caused primarily by the blowout CH_4 emissions and are not due to regular emissions in the region.

During all overpasses –albeit somewhat less pronounced on 20 April 2018–a secondary enhanced region around the city of Pittsburgh is visible, likely caused by sustained emissions due to O&G and coal mining operations in that area as suggested by EPA inventory (Fig. S8). It should be noted that the local Pittsburgh area emissions is not expected to contribute to the blowout enhancement due to the orientation of wind fields and use of *influence* mask (see Fig. 2c of main text).

Section 6: Source pixel enhancement

In Fig. 2c of the main text, we observe that the pixel containing the blowout, as well as the one immediately downwind of it, show a less pronounced XCH_4 enhancement than the pixels further downwind. This could be for a number of reasons. First, in the pixel containing the well blowout, the location of the well is half-way in the downwind direction, (see Fig. S9b) and this would cause only a partial enhancement. It is noteworthy that this low XCH_4 enhancement would not be captured by the WRF simulation as the "point source" is an evenly distributed CH_4 emission source over a WRF grid pixel of 5 km × 5 km, causing a local representation error. The TROPOMI pixel size is 7 km × 7 km at nadir. However, the pixels shown in the analysis region are 25 km wide because they are near the edge of the swath, and are thus stretched due to the large viewing zenith angle. Second, there can be a bias in the XCH_4 measurements caused by scattering of light due to simultaneously emitted liquid droplets and fine particles such as water and hydraulic fracturing fluids which can also be seen in the video of the blowout (see Movie S1). Third, the logarithmic dependence of XCH_4 on the absorption line depth would also result in an underestimate of average XCH_4 in the partially enhanced pixels. The partial pixel enhancement effect would be less significant further downwind of the source once the plume widths increases and becomes comparable to the pixel width. This is evident in the large enhancements (106±2 ppb, Fig. 1b) seen at 36 km downwind of the source. The development of a spatially dispersed plume is also evident in WRF XCH_4 (see Fig. 2a of main text).

Section 7: Total emission quantification

The uncertainty of extrapolating the blowout emission rate to the full 20-day period is difficult to assess from only a single instantaneous emission estimate derived from TROPOMI, without knowing the time dependence of the emissions. However, a range of total emission can be derived by considering a range of plausible emission rate time dependences. The gas well can be described as a pressurized chamber of finite volume leaking gas from a small orifice. For such a well, an exponentially declining emission rate during the blowout period is expected, with e-folding time equal to the ratio of the reservoir capacity and the instantaneous leakage rate. An approximately constant emission rate occurs if the leakage during the blowout period is small compared with the well capacity, i.e., e-folding time is very large compared to the blowout period. An exponential reduction has been observed in previous studies measuring emission rates from gas well blowout episodes: Conley et al. (*3*) observed exponentially decreasing emissions from the Aliso Canyon storage tank during the major portion of the ~3.5 month leakage period. Lee at al. (*4*) observed a decreasing emission rate from the uncontrolled Elgin platform gas release over a period of a month and a half, in the North Sea. Although not mentioned explicitly by Lee at al. (*4*), their measurements point to exponentially decreasing emissions.

For the Ohio blowout gas well, the pressure inside the chamber is proportional to the N moles of gas that are present as determined by the ideal gas law. Everything else kept constant, the emission rate Q is proportional to the pressure difference across the orifice. Assuming the pressure inside the well is many times larger than the atmospheric pressure outside and negligible changes in temperature, Q is given by

$$Q(t) = \frac{dN}{dt} \approx -\lambda N$$

Where λ is a constant. Using this equation, we derive the total emission E until a given time (t_c) of the blowout as a function of the ratio between initial emission rate Q_0 and the emission rate Q_t at measurement time t_m as

$$E = \frac{Q_t(1 - e^{-\lambda t_c})}{-\lambda e^{\lambda t_m}}$$

$$\lambda = \frac{\log(Q_t/Q_0)}{t_m}$$

Using these equations, the E for the Ohio blowout is shown in Fig. S10 with t_c= 20 days, t_m = 13 days and Q_t = 120 t/hr for $0.1 < \frac{Q_t}{Q_0} < 1$. Assuming a near-constant emission rate, we get a total emission of 57 kt CH_4 (or 60 ± 15 after accounting for uncertainties in the blowout emission rate). Any sustained exponential decrease in the emission rate leads to $E > 57$ kt CH_4, which means that we are likely underestimating our total emission estimate and its uncertainty.

Table S1: Uncertainty estimation due to meteorological errors derived as the sensitivity of the emission estimate to the temporal sampling of WRF.

Hour (UTC)	**Q (t/hr)**
15:00	135
16:00	93
17:00	96
18:00*	116
19:00	112
20:00	110
Standard deviation (σ_{meteo})	**14**

**Hour of WRF output used to quantify the blowout emission.*

Table S2. 10-meter wind speed averaged over the Ohio blowout region at 18:00 UTC on 27 February 2018, closest to the TROPOMI overpass time.

Meteorological Model	wind speed ± standard error (ms^{-1})
NCEP-FNL (*5*)	3.1 ± 0.3
ECMWF ERA-5 (*6*)	2.8 ± 0.1
ECMWF ERA-interim (*7*)	3.3 ± 0.1

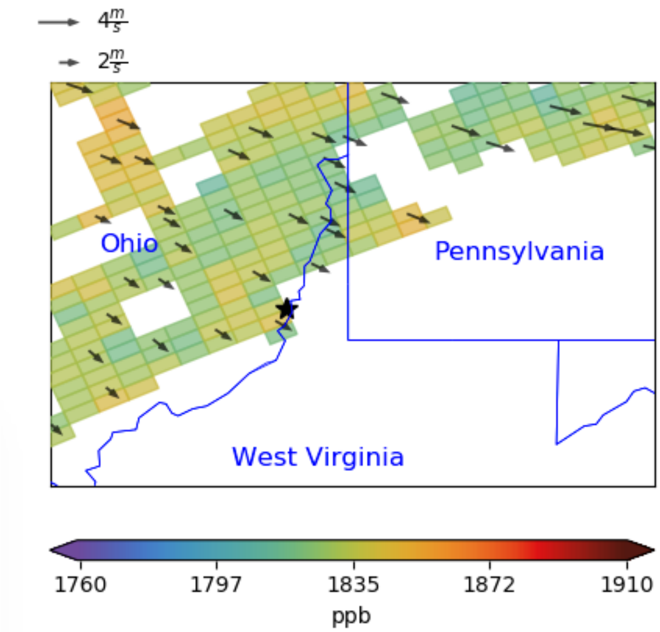

Fig. S1. As Fig. 1b in the main text but for 26 February 2018.

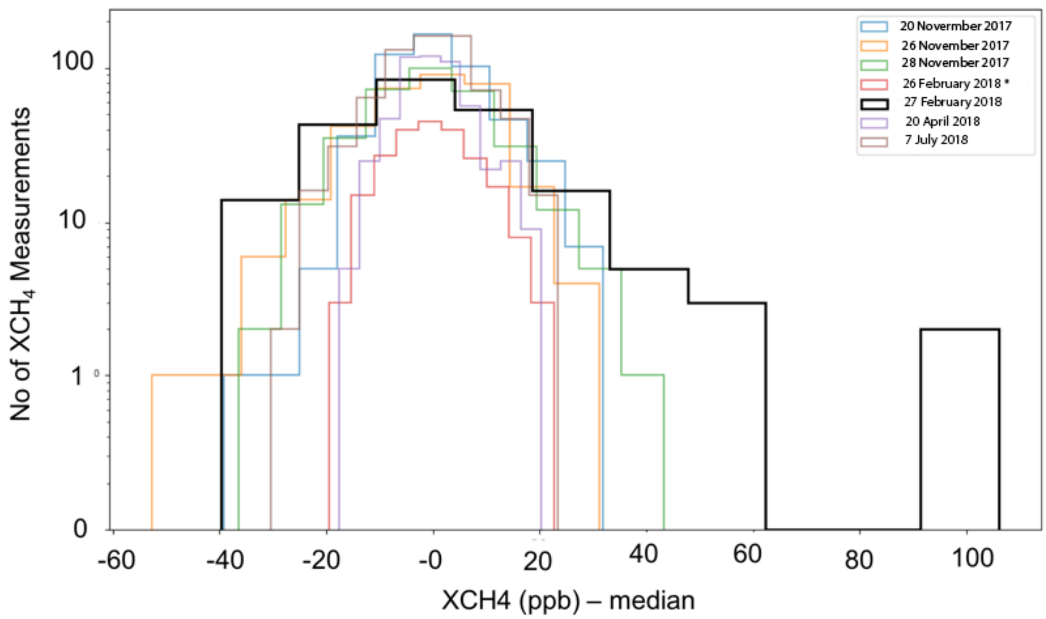

Fig. S2. Distribution of TROPOMI measurements for days with sufficient coverage in the blowout region, as shown in Fig. 1 of main text, after subtracting the median of all measurements on the respective day. Notice that the distribution of XCH_4 on 27 February 2018 (during blowout period), is positive-skewed in comparison to other days due to the large CH_4 emission from the blowout.

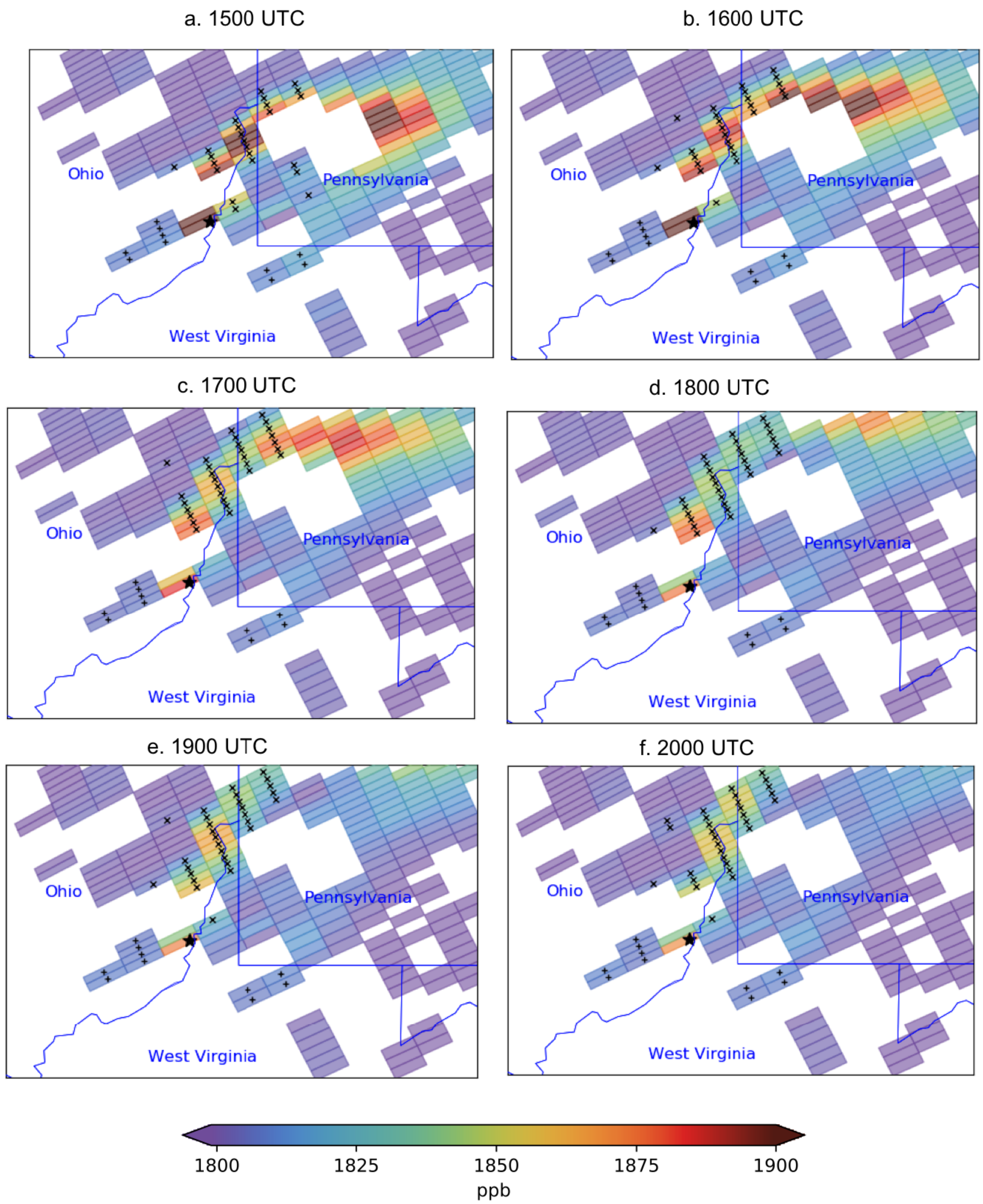

Fig. S3: WRF XCH_4 as in Fig. 2b in the main text for different hours adjacent to the TROPOMI overpass time on 27 February 2018 and the corresponding blowout-influenced (crosses) and background pixels (pluses). Note that the influence mask is different for each hour as it is calculated using the corresponding blowout tracer output.

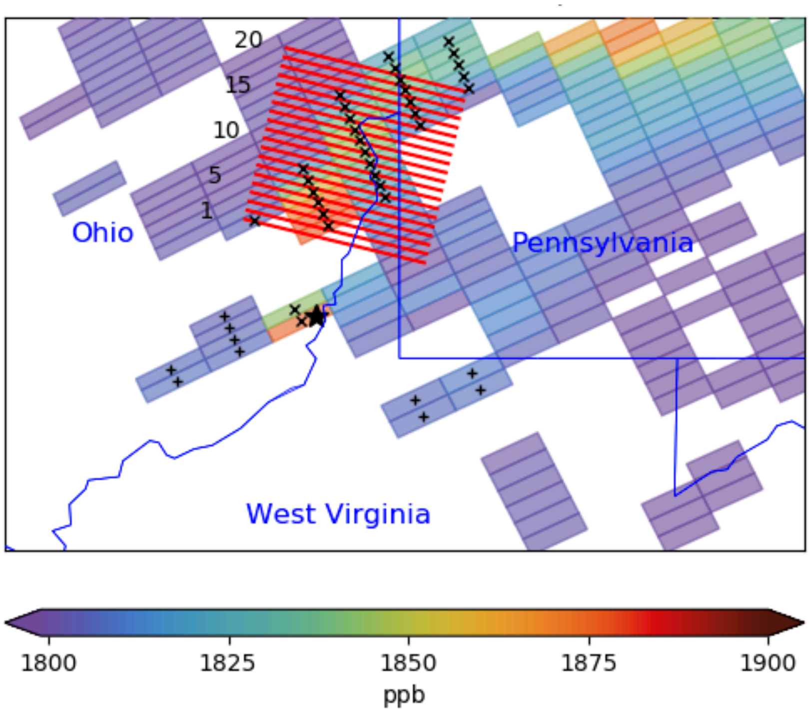

Fig. S4. As Fig. 2c of the main text, for CH_4 emission quantification using the CSF method**.** The red lines are the transect lines perpendicular to the wind direction at the blowout location. Emission estimates obtained per transect line are shown in Fig. S5.

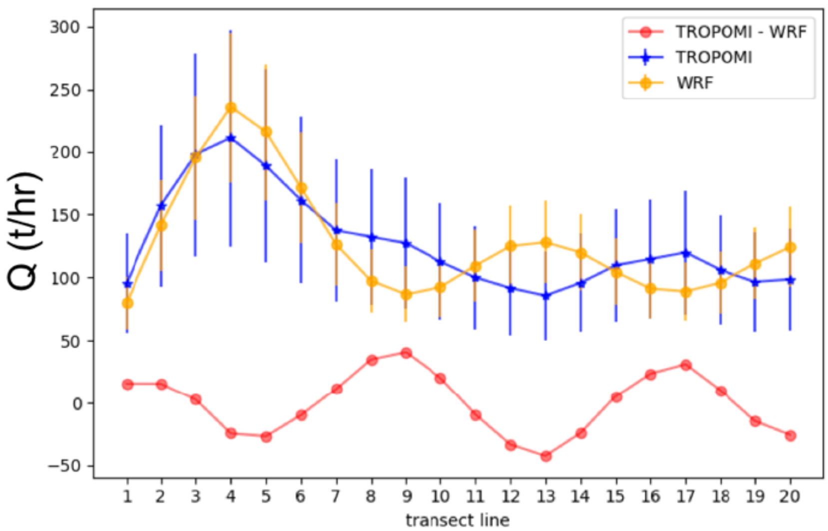

Fig S5. CH_4 emission rate, with 1 standard deviation uncertainty, calculated from TROPOMI XCH_4 along the different transect lines shown in Fig. S4 using the CSF method. WRF-derived emission rates are also plotted. Note that, to facilitate visual comparison, the WRF emission rates are multiplied by 1.62 such that their mean is equal to the mean of the TROPOM- derived emission rates.

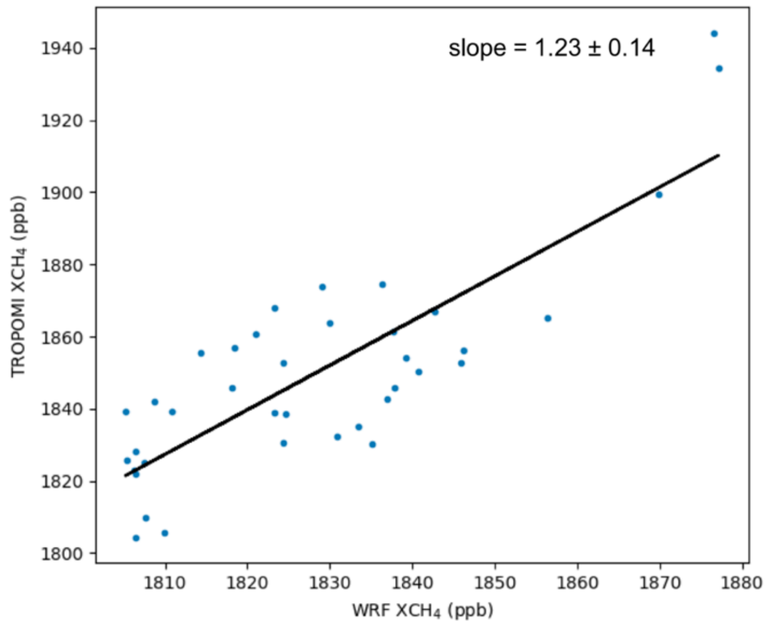

Fig. S6 TROPOMI measurements vs WRF-simulated XCH_4. Only the blowout-influenced and background pixels, marked with crosses and pluses in Figure 2c, are plotted.

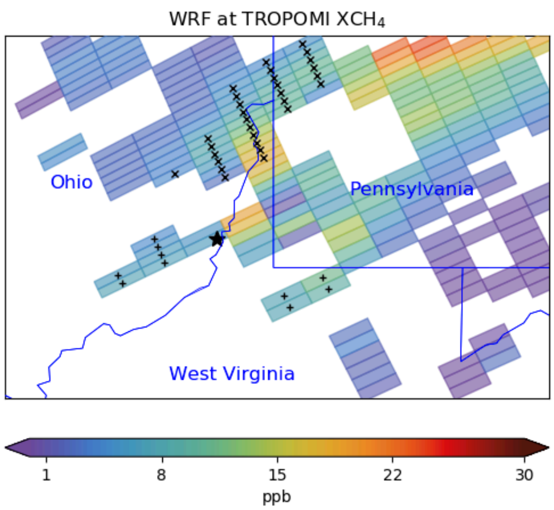

Fig. S7. WRF XCH_4 for the EPA tracer. The crosses and pluses mark the blowout-influenced and background pixels, respectively.

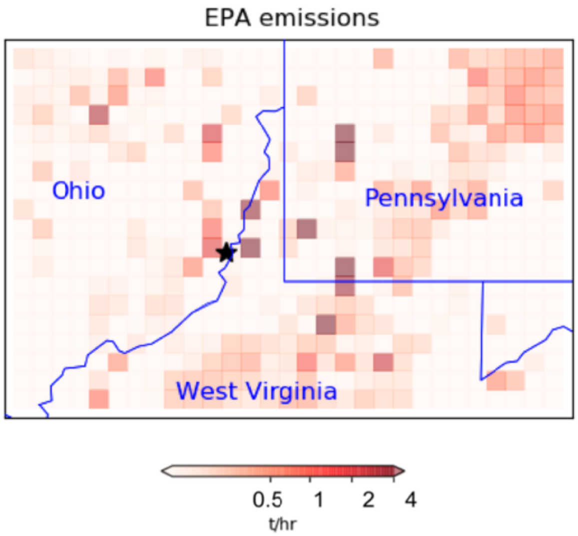

Fig. S8. Anthropogenic CH_4 emission in the blowout region for 2012 according to EPA 2012 inventory. The blowout location is marked with a black star.

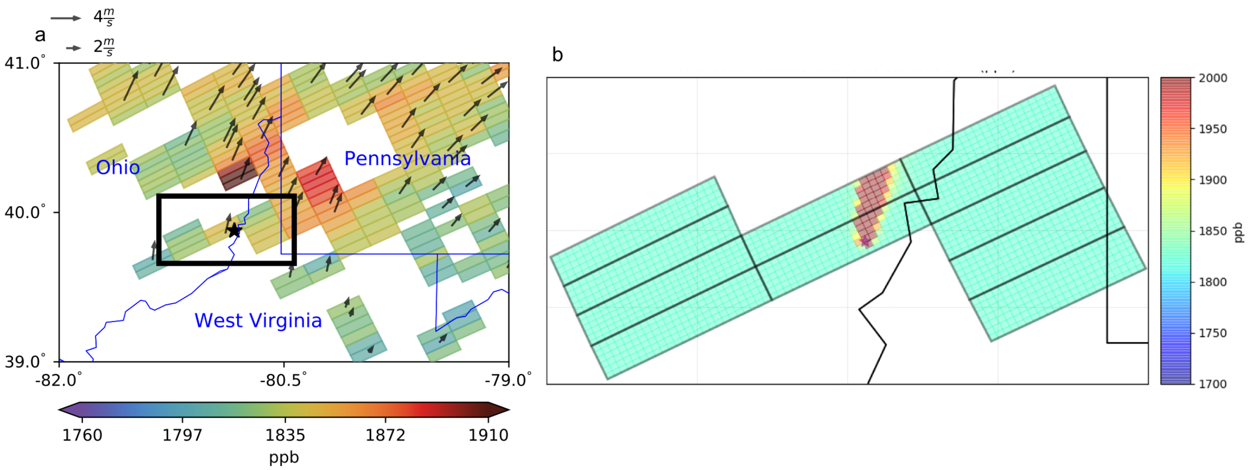

Fig S9. **Illustration of partial pixel enhancement based in a high resolution WRF run**. XCH_4 measurements (left panel; as in Fig. 1b of main text) and high resolution (1x1 km^2) WRF XCH_4 (right panel) within the TROPOMI pixels over the blowout location. The star marks the location of blowout well. The black box in the left panel shows the region that is enlarged in the right panel. The color scale of the right panel has been adjusted to facilitate the visualization of the plume.

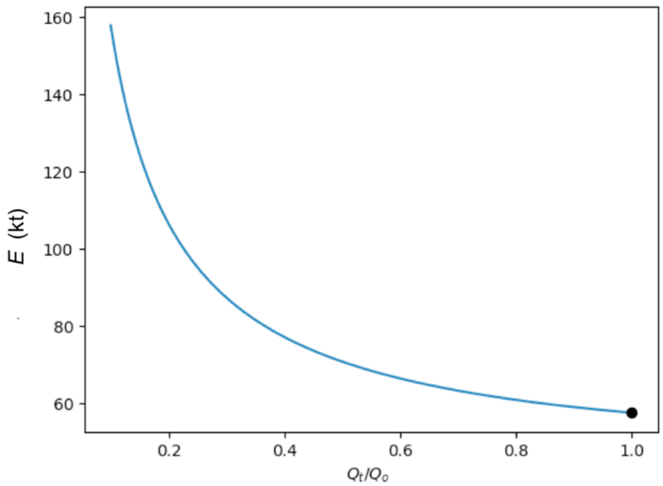

Fig. S10. Total emissions E from the Ohio blowout in 20 days as function of ratio between initial (Q_0) and measured emission rate (Q_t). If the ratio between emission rates is 1 (black dot), E = 57 kt.

Movie S1.

Movie of the leakage from the blowout on 3 March 2018 taken with FLIR (Forward Looking InfraRed) optical gas imaging cameras by Earthworks.

References

1. D. J. Varon et al., Quantifying methane point sources from fine-scale satellite observations of atmospheric methane plumes. *Atmospheric Measurement Techniques* **11**(10), 5673-5686 (2018).
2. E. A. Kort et al., Four corners: The largest US methane anomaly viewed from space. *Geophysical Research Letters* **41***,* 6898–6903 (2014). https://doi.org/10.1002/2014GL061503
3. S. Conley et al., Methane emissions from the 2015 Aliso Canyon blowout in Los Angeles, CA. *Science,* **351**, 1317–1321 (2016).
4. J. D. Lee et al., Flow rate and source reservoir identification from airborne chemical sampling of the uncontrolled Elgin platform gas release. *Atmos. Meas. Tech* **11**, 1725–1739 (2018). https://doi.org/10.5194/amt-11-1725-2018
5. National Centers for Environmental Prediction/National Weather Service/NOAA/U.S. Department of Commerce. 2000, updated daily. *NCEP FNL Operational Model Global Tropospheric Analyses, continuing from July 1999*. Research Data Archive at the National Center for Atmospheric Research, Computational and Information Systems Laboratory. https://doi.org/10.5065/D6M043C6. Accessed on 05-08-2019.
6. Copernicus Climate Change Service (C3S), “ERA5: Fifth generation of ECMWF atmospheric reanalyses of the global climate” (Copernicus Climate Change Service Climate Data Store (CDS), 2019; https://cds.climate.copernicus.eu/cdsapp#!/home) Accessed on 05-08-2019.
7. D. P. Dee et al., The ERA-Interim reanalysis: Configuration and performance of the data assimilation system. *Quarterly Journal of the Royal Meteorological Society* 137:656, 553–597 (2011).